scientific reports

Check for updates

OPEN

Cattaneo–Christov heat flow model for copper–water nanofluid heat transfer under Marangoni convection and slip conditions

Khalid Abdulkhaliq M. Alharbi[1], Mohammed Nasser Alshahrani[2], Naeem Ullah[3], Naseer M. Khan[4]✉, Krawczuk Marek[5], Abd Allah A. Mousa[6] & Sajid Ali[7]

This report is devoted to the study of the flow of MHD nanofluids through a vertical porous plate with a temperature-dependent surface tension using the Cattaneo–Christov heat flow model. The energy equation was formulated using the Cattaneo–Christov heat flux model instead of Fourier's law of heat conduction. The Tiwari–Das model was used to take into account the concentration of nanoparticles when constructing the momentum equation. The problem is described mathematically using the boundary layer approach as a PDE, which is then converted into an ODE with the help of the transformation process. The solution finding process was completed by running the bvp4c code in MATLAB. A quantitative analysis of the influence of some newly occurring parameters on physical quantities was carried out using graphics. The addition of nanoparticles to the base fluid leads to an increase in both skin friction and thermal conductivity. The increase in thermal conductivity is the advantage, while the increase in skin friction is the disadvantage of the nanoparticle concentration. Marangoni convection has proven to be one of the most cost-effective tools available that can reduce skin friction. Marangoni convection improves the heat transfer coefficient during suction but decreases the heat transfer coefficient during the injection.

The traditional Fourier law of heat transfer[1] is the most reliable approach to understanding the dynamics of heat transfer under various conditions. Nevertheless, it has a fundamental flaw: it requires the establishment of a parabolic equation for the energy of the temperature field, which is not compatible with the principle of causality. In its well-known study, Cattaneo[2] offered a successful adaptation of the Fourier model in order to add an essential feature of the thermal relaxation time. It can be seen from this that a hyperbolic energy equation is formed for a temperature field, which makes it possible to transfer heat at a limited speed via the propagation of heat waves. This type of heat transfer has interesting practical applications ranging from nanofluidic flows to modeling skin burns (it is desirable to see[3]). It has been found that thermal relaxation times for some materials, including biological tissue (1–100 s), sand (21 s), and $NaHCO_3$ (29 s), are long. To preserve the material-invariant calculation, Christov[4] replaced the time derivative with the upper-convected derivative of Oldroyd in the Maxwell-Cattaneo's model. This model is referred to in the literature as Cattaneo–Christov heat flow model. Garia[5,6] studied in detail the steady MHD flow of a hybrid nanofluid, considering multiple geometries such as wedge and cone. The natural convective boundary layer flow in the Newtonian liquid was investigated by Straughan[7]. The heat transfer study of a Maxwell fluid under the velocity slip condition according to the Cattaneo–Christov approach is carried out by Han[8]. They used methods of Homotopy analysis and a numerical method, the so-called finite difference scheme, to find solutions to the basic equations.

[1]Mechanical Engineering Department, College of Engineering, Umm Al-Qura University, Makkah, Kingdom of Saudi Arabia. [2]Department of Mathematics, College of Science and Humanities in Al-Kharj, Prince Sattam bin Abdulaziz University, Al-Kharj 11942, Saudi Arabia. [3]Department of Mathematics, Quaid-i-Azam University, 45320 Islamabad, Pakistan. [4]School of Mathematics and Statistics, Central South University, Changsha 410083, Hunan, People's Republic of China. [5]Gdansk University of Technology, Faculty of Mechanical Engineering and Ship Technology, Narutowicza 11/12, 80-233 Gdańsk, Poland. [6]Department of Mathematics and Statistics, College of Science, Taif University, P.O. Box 11099, Taif 21944, Saudi Arabia. [7]Mechanical and Energy Engineering Department, College of Engineering, Imam Abdulrahman Bin Faisal University (IAU), Dammam, Kingdom of Saudi Arabia. ✉email: nmkhan@math.qau.edu.pk

The combined effect of magnetic field and biological convection on the boundary layered flow of unsteady MHD Sakiadis and Blasius nanofluids was investigated by Ali[9]. Ibrahim[10] published a communication report on viscoelastic nanofluid flow related to the Cattaneo–Christov mass and heat flow model and third-order velocity slip, and investigated various relevant flow parameters. Using a new mathematical model of a second-grade bio-convective nanofluid in combination with viscous dissipation and the Cattaneo–Christov heat flow model for the transfer of heat through a permeable medium, Raja[11] initiated a study with the Levenberg-Marquardt technique (LMT) on the smooth backpropagated Neural Networks (BNN) calculation. The effect of MHD on the rotational flow of the unsteady Oldroyd-B nanofluid with the concentration and temperature of the nanoparticles is related to Brownian motion and the Cattaneo–Christov heat flow is explained by Ali[12]. With the Cattaneo–Christov heat flow, the VON Kármán spinning flow problem is extended to the slip condition of Navier on the stretched spinning disk surface. Lim[13] examined semi-analytically the flow of an MHD Casson liquid over a rotating disk. Farooq's research is aimed at obtaining numerical results for an MHD nanofluid flow with a Cattaneo–Christov heat flow model and thermal radiation through a stretched surface with melting boundary conditions. The Cattaneo–Christov model is used for a 2D boundary layer. Salahuddin's study[14] uses the nanofluid cross-flow across the surface of a parabola and the temperature-dependent viscosity to investigate heat and mass diffusion. In addition, the study of the influence of changes in enthalpy and activation energy broadens the scope of this topic. Mushtaq[15] considered the Cattaneo model, which is an improved form of the Fourier equation for heat conduction, including thermal inertia.

When surface tension is high due to temperature and material gradients, Marangoni convection occurs. Microgravity is dominated by Marangoni convection and its applications include heat exchangers, crystal growth, coating processes, soap film stabilization, silicon wafer growth and other technical applications[16]. Using a series of three-dimensional numerical calculations that take into account the effect of radiative heat transfer to the free surface, the properties of Marangoni convection in a shallow rectangular cavity subject to mutually perpendicular gradients of temperature and concentration are investigated[17–21]. Wang[22] experimentally investigated the tendencies of Marangoni convection in an evaporating droplet deposited over a volatile liquid layer. At two different equilibrium states, two types of Marangoni instabilities are found on the surface of a methanol droplet. In the entire floating zone with radiant heat transfer under zero gravity conditions, Chihao Jin[23] carried out a computational study of the Marangoni thermosolar convection. Sun[24] has developed an axisymmetric 2D mathematical model to predict the melting of spherical EPCMs, including air pockets at the top. In addition to natural convection due to buoyancy, this topic also discusses for the first time Marangoni convection due to thermocapillary force at the PCM interface with molten air. The entropy nature of the laminar, steady, relative contribution of solitary and thermal Marangoni convection during the passage of a hybrid Cassonian nanofluid (Al_2O_3-Cu-H_2O) in a disk flow under the action of a nonlinear heat source/sink, radiation, viscous dissipation and nonlinear convection are described in the Yun-Xiang Li's[25] study.

Microfluidics, semiconductor vapor drying in microelectronics, foams, surfactant replacement therapy for newborns, coating technology and film drainage in emulsions are examples of Marangoni convection, which is important in industrial, biomedical and everyday applications. Song's[26] research focuses on the role of bio-convection in the flow of Carreau nanofluid through a stretched cylinder. The study was modified to include the effects of melting and chemical reactions. Zhang[27] used a series of 3D numerical models to study the features of Marangoni convection in a narrow rectangular channel with a linear boundary condition. In his work, Mackolil[28–33] explains many aspects of Marangoni convection on the macroscopic properties of nanofluids by considering different geometries with new boundary conditions and fluid models. Kazemi[34] developed a study to investigate the formation of entropy in hybrid nanofluids, including parts of Marangoni convection and a Darcy-Forchheimer model to explain the momentum equation.

In the current study, the authors examined the flow of a viscous nanofluid on a vertical porous plate with the effects of the magnetic field, suction, and Cattaneo–Christov heat flux. The effect of Marangoni convection and volume fraction during heat transfer was investigated using the Tiwari–Das model and the Cattaneo–Christov model. Many scientists, including Farooq[35], have worked on a comparative problem of fluid flow through a vertical porous plate, but none have related Marangoni convection and Cattaneo–Christov heat flow in their research. When the Cattaneo–Christov heat flow and slip conditions are included, fluid problems are appropriately addressed in the real scenario. The assumption that a liquid flows through a porous plate is critical to many industrial and technological activities, including power generation, turbomachinery, and food processing. The stated purpose of the analysis is:

- The equations of concentration and energy are modified using the connections of the Cattaneo–Christov theory.
- The purpose of this study is to see how Marangoni convection affects the thermal transport of nanofluid.
- To see how velocity slip affects the thermal transport of nanofluid.
- The effect of the Prandtl number on the effective Prandtl method, as well as the suction phenomenon, was investigated.
- The concentration, velocity and temperature of the nanofluid are analyzed using 2D graphical analysis.

Mathematical modeling

In the Cartesian plane, it is proposed to study the Marangoni convection of Copper–Water MHD nanofluids with temperature-dependent surface tension and Cattaneo–Christov heat flux. The flow at the surface of a porous vertical plate is considered under the assumption that there is a constant suction v_0 at the surface. Suction is a boundary layer control approach aimed at reducing energy losses in channels or drag on bodies in an external flow. The nanofluid investigated was prepared by immersing copper nanoparticles in water and was called the

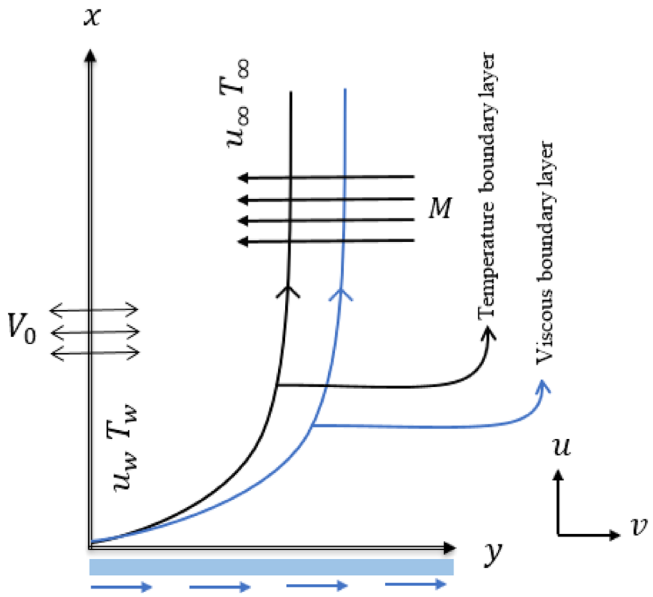

Figure 1. Flow model exhibition.

Tiwari–Das model[36] for constructing the equation of momentum. The nanofluid flow is magnetized by passing a constant magnetic flux perpendicular to the nanofluid flow (see Fig. 1). Due to the low Reynolds number, the strength of the induced magnetic field is negligible and the induced magnetic field does not affect heat transfer. The current study assumes that the viscosity and density of the fluid are independent of temperature. The velocity of nanofluid is zero if the distance from the sheet is significant and the temperature at this point is considered equal to T_∞, and the surface temperature of the sheet is expressed as T_w. The momentum and temperature equations that govern the current flow model can be approximated by boundary layer approximation as follows[37,38]:

$$\frac{\partial u}{\partial x}+\frac{\partial v}{\partial y}=0, \tag{1}$$

$$u\frac{\partial u}{\partial x}+v\frac{\partial u}{\partial y}=\left(\frac{\mu}{\rho}\right)_{nf}\frac{\partial^2 u}{\partial y^2}-\left(\frac{\sigma}{\rho}\right)_{nf}{B_0}^2 u, \tag{2}$$

$$\begin{aligned} u\frac{\partial T}{\partial x}+v\frac{\partial T}{\partial y}=\alpha_{nf}\frac{\partial^2 T}{\partial y^2}-\lambda_T\Bigg(&u^2\frac{\partial^2 T}{\partial x^2}+v^2\frac{\partial^2 T}{\partial y^2}+2uv\frac{\partial^2 T}{\partial x\partial y}+u\frac{\partial u}{\partial x}\frac{\partial T}{\partial x}\\ &+u\frac{\partial v}{\partial x}\frac{\partial T}{\partial y}+v\frac{\partial u}{\partial y}\frac{\partial T}{\partial x}+v\frac{\partial v}{\partial y}\frac{\partial T}{\partial y}\Bigg), \end{aligned} \tag{3}$$

The Cartesian velocity components in the x- and y- directions are indicated as u and v, respectively. Thermal diffusivity of nanofluid is represented as α_{nf}, density is represented as ρ_{nf}, and dynamic viscosity is represented as μ_{nf}. The indices f and nf indicate the base fluid and nanofluid. The thermal relaxation time of the fluid is specified by λ_T. The main thermophysical properties of the nanofluids investigated are taken from the standard literature. The combination of equations that can estimate the physical aspects of the flow model is related to the following boundary conditions:

$$\left.\begin{aligned} &\mu_{nf}\frac{\partial u}{\partial y}=-N\frac{\partial \sigma_m}{\partial x}=-N\frac{\partial \sigma_m}{\partial T}\frac{\partial T}{\partial x}, v=v_0, T=T_w=T_\infty+T_0\left(\frac{x}{l}\right)^2 \text{ at } y=0,\\ &[5pt]u\longrightarrow 0, v\longrightarrow 0, T\longrightarrow T_\infty \text{ as } y\longrightarrow\infty. \end{aligned}\right\} \tag{4}$$

The coefficient of surface tension, which is a function of temperature, can be formulated by the following equation[39]:

$$\left.\begin{aligned} &\sigma_m=\sigma_0[1-\gamma_T(T-T_\infty)],\\ &\gamma_T=\frac{-1}{\sigma_0}\frac{\partial \sigma_m}{\partial T}|_{T=T_\infty}. \end{aligned}\right\} \tag{5}$$

The parameters occurring in the boundary conditions can be explained by the fact that N is the slip coefficient, σ_m is the surface tension and l is the characteristic length. The following are the Similarity Transformations used in this article to convert the partial differential equations to regular ordinary ones[37].

$$\left.\begin{aligned} u = axf'(\eta), v = \left(av_f\right)^{\frac{1}{2}} f(\eta), \\ T = T_\infty + (T_w - T_\infty)\theta(\eta), \eta = \left(\frac{a}{v_f}\right)^{\frac{1}{2}} y. \end{aligned}\right\} \tag{6}$$

The continuity equation is satisfied by applying the transformation defined above while converting the momentum and temperature equations into the following equations.

$$\frac{\rho_f}{\rho_{nf}}\frac{\mu_{nf}}{\mu_f} f''' + ff'' - (f')^2 - \frac{\sigma_{nf}}{\sigma_f}\frac{\rho_f}{\rho_{nf}} Mf' = 0, \tag{7}$$

$$\frac{k_{nf}}{k_f}\theta'' + \frac{(\rho c_p)_{nf}}{(\rho c_p)_f} Pr\left[\left(f\theta' - 2f'\theta\right) + \lambda_1\left(5ff'\theta' + 2ff''\theta - \theta(f')^2 - f^2\theta''\right)\right] = 0. \tag{8}$$

Boundary conditions are transformed as follows:

$$\left.\begin{aligned} f(0) = S, f''(0) = -2\lambda Ma(1-\phi)^{(-2.5)}, \theta(0) = 1, \\ f' \longrightarrow 0, \theta \longrightarrow 0, \text{ as } \eta \longrightarrow \infty. \end{aligned}\right\} \tag{9}$$

The dimensionless parameters involved in Eqs. (7)–(9) are mathematically represented as:

$$\left.\begin{aligned} M = \frac{2\sigma_f {B_0}^2}{\rho_f a}, Pr = \frac{(\mu c_p)_f}{k_f}, Ma = \frac{\gamma_T \sigma_0 T_0}{l^2 a\sqrt{a\rho_f \mu_f}}, \lambda_1 = a\lambda_T, \\ S = v_0(cv)^{-\frac{1}{2}}, \lambda = a\sqrt{\frac{U_0}{N}} \end{aligned}\right\} \tag{10}$$

Numerical procedure

By including similarity variables, the corresponding partial differential equations and boundary conditions are first converted into a set of non-linear ordinary differential equations. The Eqs. (7), (8) and the boundary conditions (9) are then transformed into a system of ordinary differential equations of the first order, which are numerically solved in MATLAB using the bvp4c approach. The collocation approach has been used to solve the following problem. The procedure is explained as follows. Let $f(\eta) = s_1, f'(\eta) = s_2, f''(\eta) = s_3, \theta(\eta) = s_4, \theta'(\eta) = s_5$. Then the set of equations written at the last of the mathematical modeling section as:

$$ss_1(\eta) = \frac{\rho_{nf}\mu_f}{\rho_f\mu_{nf}}\left[(s_2)^2 + \frac{\sigma_{nf}}{\sigma_f}\frac{\rho_f}{\rho_{nf}} Ms_2 - s_1 s_3\right] \tag{11}$$

$$\begin{aligned} ss_2(\eta) = & \frac{-Pr(\rho c_p)_{nf}}{\left[\frac{k_{nf}}{k_f} - \frac{{s_1}^2 Pr(\rho c_p)_{nf}}{(\rho c_p)_f}\right](\rho c_p)_f}\left[(s_1 s_5 - 2s_2 s_4) + \lambda_1(5s_1 s_2 s_5 + 2s_1 s_3 s_4\right. \\ & \left.-s_4(s_2)^2)\right] = 0. \end{aligned} \tag{12}$$

$$\left.\begin{aligned} s_1(0) = S, s_3(0) = -2\lambda Ma(1-\phi)^{(-2.5)}, s_4(0) = 1, \\ [5pt] s_2 \longrightarrow 0, s_4 \longrightarrow 0, \text{ as } \eta \longrightarrow \infty. \end{aligned}\right\} \tag{13}$$

To find a solution, you need to run a residual test for accurate data transfer and grid-point selection when working with the bvp4c scheme in MATLAB. The convergence criterion for this particular numerical code is 1×10^{-6}. Dividing the difference between the edge points by the number of grid points gives the step size (i.e. $\frac{b-a}{n}$). If one of the boundary points is infinite, you must use the corresponding integer. In this case, the value $\eta = \eta_\infty = 10$ was used. Make good initial estimates to find the best solution to the Eqs. (11), (12) and related boundary condition problems.

Discussion

In this part, the influence of the corresponding parameters of the problem being solved on temperature and speed is investigated. To do this, some images are created by changing the value of a parameter in a certain range, and other parameters such as: $A(=\frac{\rho_f\mu_{nf}}{\rho_{nf}\mu_f}) = 0.5$, and $B(=\frac{\sigma_{nf}\rho_f}{\sigma_f\rho_{nf}}) = 0.4$, $k_1(=\frac{k_{nf}}{k_f}) = 0.1$, $\tau(=\frac{(\rho c_p)_{nf}}{(\rho c_p)_f}) = 0.5$, $Pr = 6.0674$ (for water Pr = 6.0674), $\lambda_1 = 0.5, S = 0.5$, Ma= 0.8, and $\phi = 0.05$ are unchanged. We found that the results are consistent and have significant parallels with previous work (see Table 1), assuming that the flow model is physically stable and the numerical solution method, in particular the "bvp4c" scheme, is correct. Table 2 shows the main thermophysical properties of the base fluid and nanoparticles[40]. Figures 2, 3, 4, 5, 6 and Table 1 are constructed using the bvp4c MATLAB code provided in Appendix A.

Figure 2a shows the behavior of the velocity as a function of η when the magnetic parameter is changed in a certain range. The figure above shows that the increase or decrease in velocity occurs in a pattern opposite to the magnetic parameter. The physical reason is that the liquid particles are attracted by the opposite Lorentz force, which causes the liquid particles to move slowly. As a result, the overall fluid velocity decreases. Fig. 2a shows the behavior of the velocity as a function of η when the magnetic parameter changes in three-dimensional space. The Fig. 3c shows how the Marangoni convection parameter (Ma) affects fluid velocity without changing

Pr	7.0	10	15
Isak et al.[41]	0.8086	1.0000	1.9237
Ganesh et al.[42]	0.808631	1.000000	1.923682
Umar et al.[35]	0.808631	1.000000	1.923682
Current results	0.808630	1.000000	1.923677

Table 1. Comparison of the results by calculating $-\theta'(0)$ values for different Prandtl numbers.

	$C_p\left[\frac{\mathrm{J}}{\mathrm{K\,kg}}\right]$	$\rho\left[\frac{\mathrm{kg}}{\mathrm{m^3}}\right]$	$k\left[\frac{\mathrm{W}}{\mathrm{K\,m}}\right]$	$\beta \times 10^5\left[\frac{1}{\mathrm{K}}\right]$
Cu (copper)	385	8933	401	1.67
H_2O (pure water)	4179	997.1	0.613	21

Table 2. Thermophysical properties of water and copper.

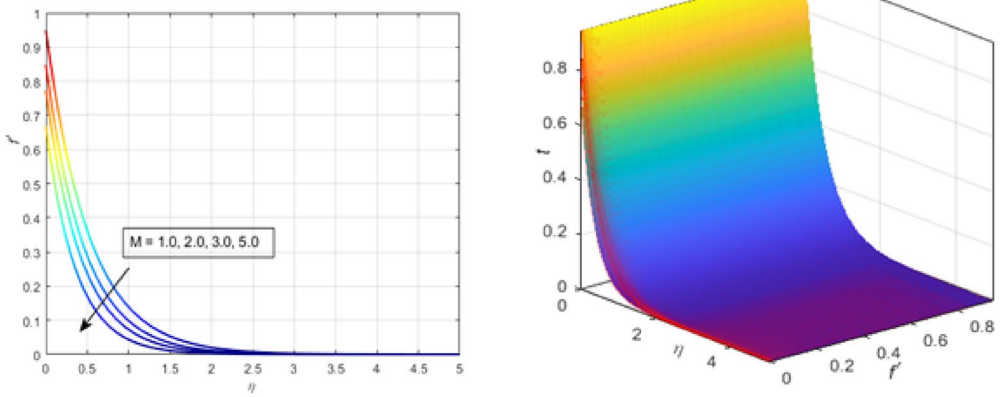

(a) Demonstration of "velocity verses magnetic parameter"

(b) Demonstration of "velocity verses magnetic parameter" in 3D

Figure 2. Demonstration of the dependence of velocity on the physical parameters in both 2D and 3D (see Appendix A).

all other parameter values. It is noted that the velocity profile changes in the same way as the parameter Ma. The speed increases when this parameter is increased, and slows down when the Marangoni convection parameter (Ma) decreases. The surface tension gradient in liquids is often associated with Marangoni convection. As the Marangoni convection parameter increases, these surface tension gradients develop and liquid particles on the surface rapidly flow into regions of low surface energy. In other words,, the higher the Ma, the lower the viscosity. The smaller the viscous force, the faster the fluid velocity. The Fig. 3d shows the behavior of the velocity as a function of η with a change in the Marangoni convection parameter in three-dimensional space.

The behavior of the speed as a function of η with a change in the concentration of nanoparticles (ϕ) in a certain range is shown in Fig. 3e. It should be noted that the velocity values are lower for a concentrated suspension of nanoparticles. A concentrated suspension is more likely to cause collisions between liquid particles. The speed of the particles decreases after colliding with another particle, which causes the speed of the liquid on the graph to decrease. Figure 3f shows the behavior of the velocity as a function of η with a change in the concentration of nanoparticles in three-dimensional space. Figure 3a shows a graph of velocity versus suction for two different cases of velocity slip, with all other parameters remaining unchanged. As expected, the velocity was found to be a decreasing function of the suction parameter. Suction, in physical terms, refers to the flow of fluid from a region of low pressure to a region of high pressure. It is quite clear that the liquid decreases as it enters the region of high pressure from the region of low pressure. The Fig. 3b shows the behavior of the velocity as a function of η when changing the suction parameter in three-dimensional space.

The curve of the temperature dependence on the magnetic parameter with all other parameters fixed is shown in Fig. 4a. When electromagnetic waves flow through the liquid, the particles vibrate with a higher frequency, increasing the kinetic energy of the particles. Due to the direct relationship between kinetic energy and

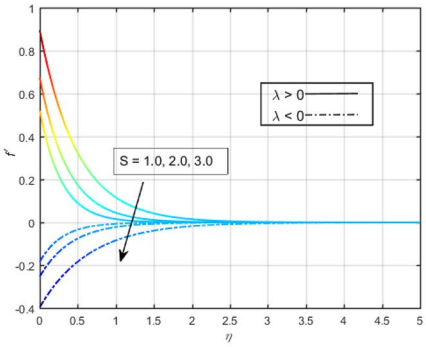

(e) Demonstration of "velocity verses suction parameter"

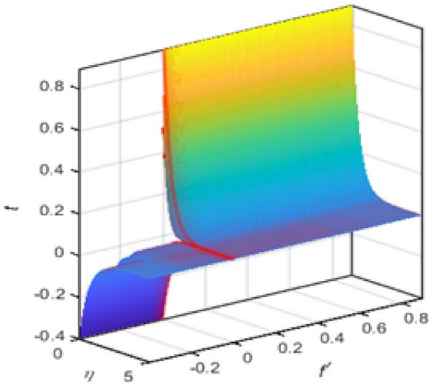

(f) Demonstration of "velocity verses suction parameter" in 3D

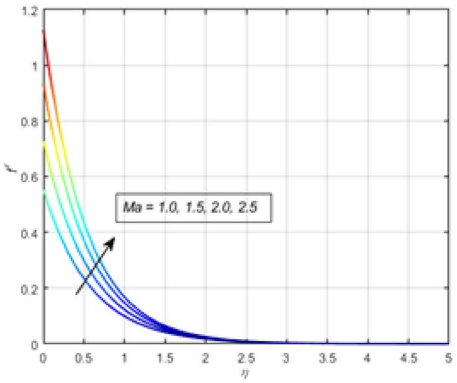

(a) Demonstration of "velocity verses Marangoni convection parameter"

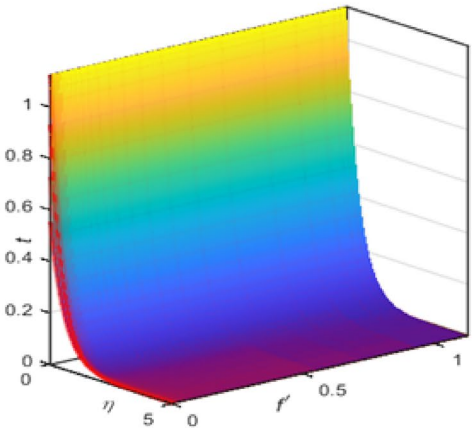

(b) Demonstration of "velocity verses Marangoni convection parameter" in 3D

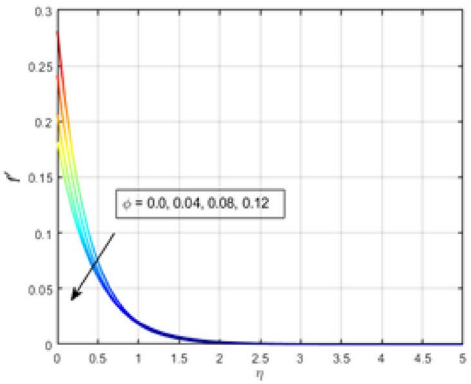

(c) Demonstration of "velocity verses nanoparticles concentration"

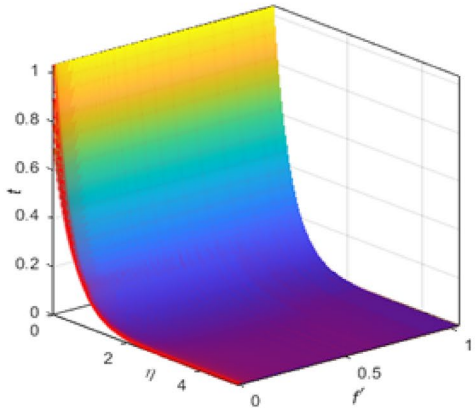

(d) Demonstration of "velocity verses nanoparticles concentration" in 3D

Figure 3. Demonstration of the dependence of velocity on the physical parameters in both 2D and 3D (see Appendix A).

temperature, the temperature of the liquid rises. Figure 4b shows the behavior of temperature depending on η when changing the magnetic parameter in three-dimensional space.

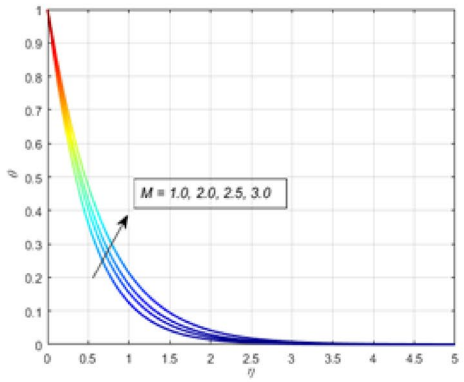

(a) Demonstration of "temperature verses Magnetic parameter"

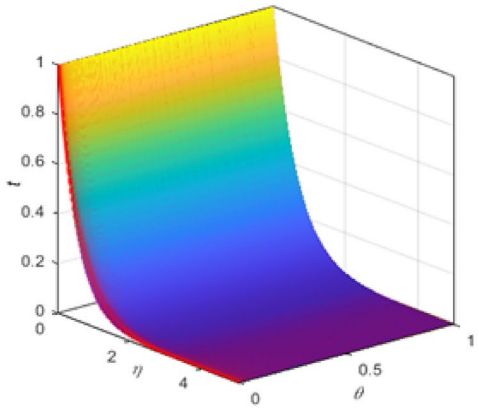

(b) Demonstration of "temperature verses Magnetic parameter" in 3D

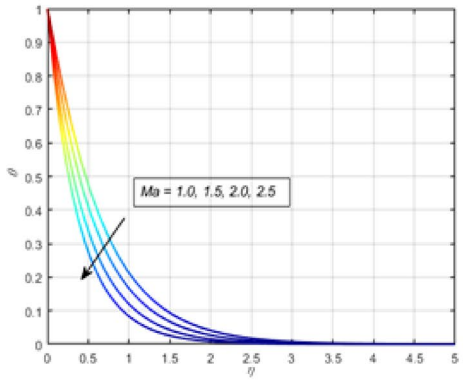

(c) Demonstration of "temp. verses Marangoni convection parameter"

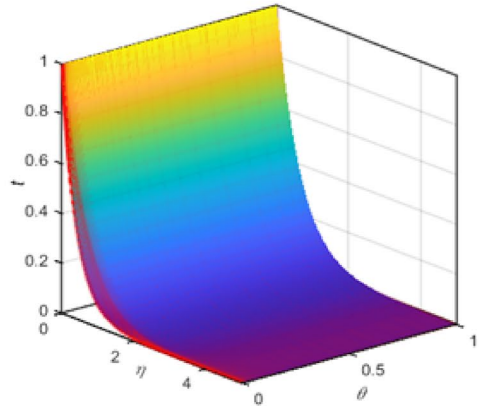

(d) Demonstration of "temp. verses Marangoni convection parameter" in 3D

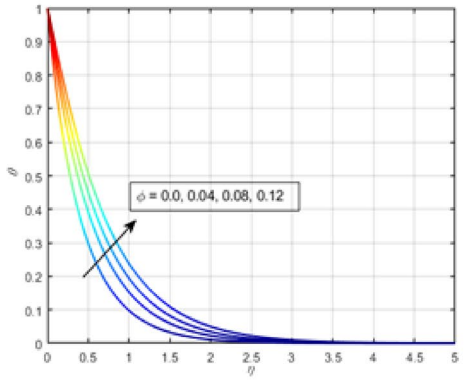

(e) Demonstration of "temp. verses concentration of nanoparticles"

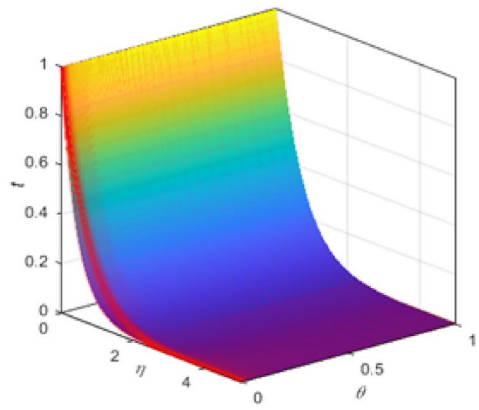

(f) Demonstration of "temp. verses concentration of nanoparticles" in 3D

Figure 4. Demonstration of "temperature verses different physical parameters" (see Appendix A).

Figure 4c shows the temperature dependence on the Marangoni convection parameter when all other parameters remain constant. The temperature profile is reduced due to the Marangoni convection parameter, as seen

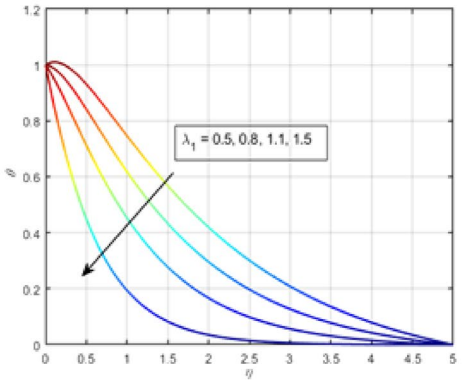

(a) Demonstration of "temperature verses slip parameter"

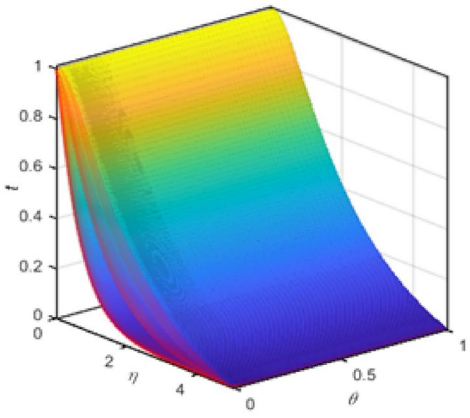

(b) Demonstration of "temperature verses slip parameter" in 3D

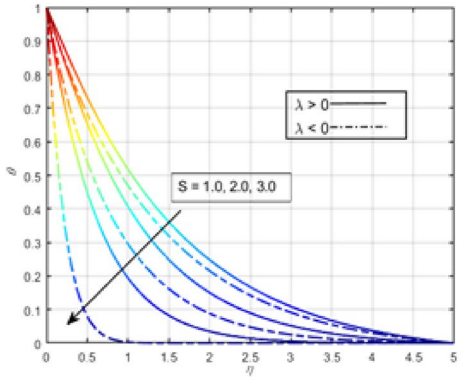

(c) Demonstration of "temperature verses suction parameter"

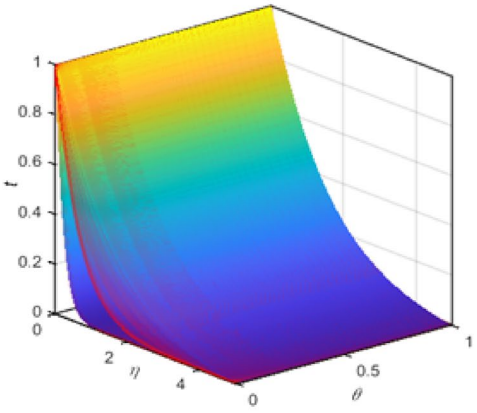

(d) Demonstration of "temperature verses suction parameter" in 3D

Figure 5. Exhibition of the influence of physical parameters on physical quantities (see Appendix A).

in the figure below. Undoubtedly, the speed increases as the viscosity decreases for larger values of Ma. The average kinetic energy of fluid particles is defined as temperature. Therefore, the higher the Ma, the higher the temperature. Figure 4d shows the behavior of temperature as a function of η when changing the parameter of Marangoni convection in three-dimensional space. Figure 4e shows the relationship between temperature and nanoparticle concentration, while all other factors remain constant. As you can see in the diagram below, increasing the concentration of nanoparticles improves the temperature profile. This is because when the dispersion of nanoparticles is concentrated, the nanoparticles are more prone to collisions. The temperature of the liquid rises as a result of the huge number of collisions between the nanoparticles. Figure 4f shows the behavior of temperature as a function of η when changing the concentration of nanoparticles in three-dimensional space. The dependence of the temperature curve on λ_1 (thermal relaxation parameter) with all other parameters rigidly set was tested in Fig. 5a. The thermal relaxation parameter tends to decrease the temperature curve, which can be seen in the figure. Figure 5b shows the behavior of temperature as a function of η when changing the thermal relaxation parameter in three-dimensional space.

The dependence of the temperature curve on the suction parameter with a rigid setting of all other parameters was tested in Fig. 5c. A decrease in the temperature curve was observed at a high surface suction resolution. Suction has a physical effect on temperature because heat transmission increases as suction on the surface increases. The temperature drops as heat is quickly transmitted from one spot to another. Figure 5d shows the behavior of temperature as a function of η when changing the suction parameter in three-dimensional space.

The effect of the Marangoni convection parameter on skin friction by leaving all other parameters unchanged is shown in the Fig. 6a. The Marangoni convection parameter is able to reduce the skin friction coefficient, as can be seen from the attached figure. Figure 6b shows the behavior of the skin friction curve for different values of nanoparticle concentration, keeping the remaining parameters constant. The frictional force between a solid and a liquid is physically referred to as skin friction. In the case of a concentrated suspension of nanoparticles, the interaction of a solid with a liquid is significant and therefore the coefficient of skin friction increases.

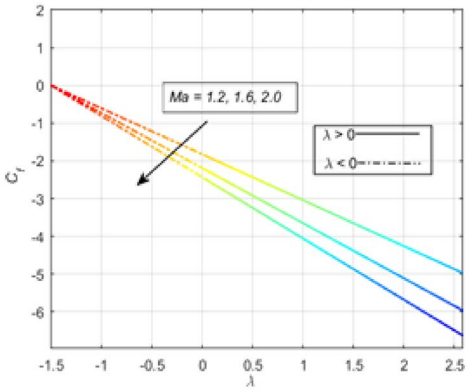

(a) Demonstration of "skin friction verses Marangoni convection parameter"

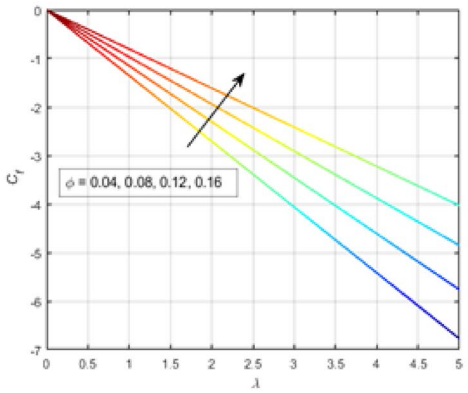

(b) Demonstration of "skin friction verses Marangoni convection parameter"

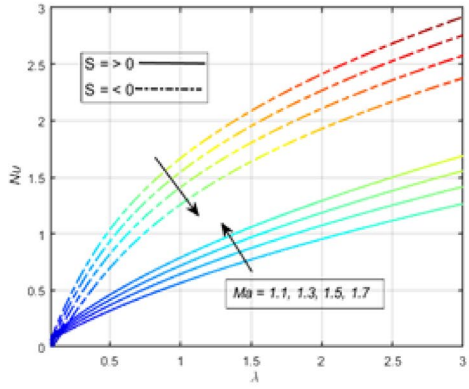

(c) Exhibition of "Nusselt number verses Marangoni convection parameter"

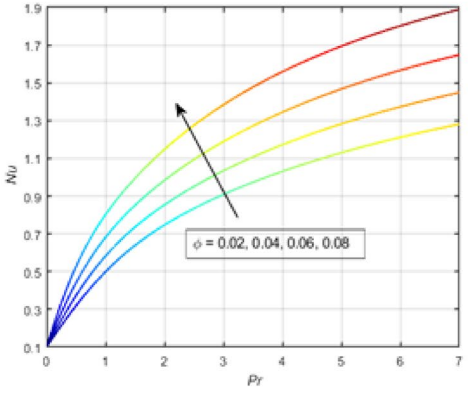

(d) Exhibition of "Nusselt number verses concentration of nanoparticles"

Figure 6. Exhibition of the influence of physical parameters on physical quantities (see Appendix A).

The Nusselt number was tested for different values of the Marangoni convection parameter for suction and injection separately in Fig. 6c. The Marangoni convection parameter promotes the Nusselt number during surface suction and lowers the temperature during surface injection. The Nusselt number was tested for various values of the concentration of nanoparticles, the rest of the parameters were set fixed in Fig. 6d. A suspension of nanoparticles has a tremendous ability to transfer heat in the case of a concentrated suspension. The physical reason is that the addition of nanoparticles improves the thermal conductivity of the liquid. Since there is a large amount of coolant, this leads to an increase in the Nusselt number.

Conclusion

The Cartesian plane has been used to study the Marangoni convection of non-Newtonian MHD nanofluids with temperature-dependent surface tension and Cattaneo–Christov heat flux. Similarity variables were used to transform ruling PDEs to regular ordinary equations. Since bvp4c is a numerical code for a computationally intensive solution, it is used here to track the solution of the developed model. The dependence of some important physical quantities such as speed, skin friction, temperature and Nusselt number on some new physical parameters was checked. Excellent convergence and consistency was found when comparing the results with the previous publication and therefore we can argue that bvp4c is a computational code that is executed with very little effort.

- A direct relationship was found between the fluid velocity and the Marangoni convection parameter, and the inverse relationship was found between the temperature and the Marangoni convection parameter.
- The purpose of the implantation of the magnetic field is to balance the suction rate, which results in a decrease in fluid velocity.
- One of the main goals of this study is to reduce skin friction. Marangoni convection has been found to be one of the inexpensive tools available that can reduce skin friction.
- The advantage of nanoparticle concentration is that it improves the thermal conductivity of the nanofluid, but on the other hand it significantly increases the skin friction. This is a drawback of the high concentration of nanoparticles.

- If there is suction on the surface, the Marangoni convection setting will greatly improve the heat transfer coefficient, but in the case of injection it will tend to lower the heat transfer coefficient.
- The higher the concentration of nanoparticles, the higher the heat transfer rate will be and vice versa.

Appendix A

```
function
clc;
% Author: NM Khan
% Physical Parameters
A = 0.5; B = 0.4; k1 = 0.1; tau = 0.5; Pr =6.0674; lambda1 = 0.5; lambda = 0.5; S=0.5; Ma= 0.8, phi= 0.05
% Initial guess
sol = bvpinit(linspace(0,5,100), [0 0 0 0 0]);
% solution in structure form
sol1 = bvp4c( bvpexam2, bcexam2, sol);
lastwarn(' new_msgstr ');
% x values
x1 = sol1.x;
% s values in row form (s, s', s'', theta, theta')
s1 = sol1.s;
% plot any one of the solutions s1, here we plot theta figure (1)
plot(x1, s1(2, :), ' b ', ' linewidth ', 1, ' Linesmoothing', ' on');
xlabel(' \eta ')
ylabel(' \f ^{\prime} (\eta) ')
% grid on
hold all
value = deval(sol1, 0);
% get results upto six digits
vpa(value, 6)
hold on
% Here I define residual of boundary conditions
function res = bcexam2(s0, sinf)
res = [s0(1) - S; s0(2) + 2 * lambda * Ma * (1 - phi) ^(-2.5); s0(4) - 1; sinf(2); sinf(4)];
end
% First order ODEs are define here
function ysol = bvpexam2(x,s)
ss1 = (1/A)(-s(1) * s(3) + s(2) ^2 + B * M * s(2));
ss2 = -(1/(k1 - tau * Pr * s(1)
^2))*tau*Pr*(s(1)*s(5)-2*s(2)*s(4)+lambda1*(5*s(1)*s(2)*s(5)+2*s(1)*s(3)*s(4)-s(2) ^2 * s(4)));
ysol = [s(2); s(3); ss1; s(5); ss2];
end
end
```

Received: 15 January 2022; Accepted: 21 March 2022
Published online: 30 March 2022

References

1. Grattan-Guinness, I. Joseph fourier, théorie analytique de la chaleur (1822). In *Landmark Writings in Western Mathematics 1640–1940*, 354–365 (Elsevier, 2005).
2. Cattaneo, C. Sulla conduzione del calore. *Atti Sem. Mat. Fis. Univ. Modena* **3**, 83–101 (1948).
3. Tibullo, V. & Zampoli, V. A uniqueness result for the Cattaneo–Christov heat conduction model applied to incompressible fluids. *Mech. Res. Commun.* **38**(1), 77–79 (2011).
4. Christov, C. I. On frame indifferent formulation of the Maxwell-Cattaneo model of finite-speed heat conduction. *Mech. Res. Commun.* **36**(4), 481–486 (2009).
5. Garia, R., Rawat, S. K., Kumar, M. & Yaseen, M. Hybrid nanofluid flow over two different geometries with Cattaneo–Cristov heat flux model and heat generation: A model with correlation coefficient and probable error. *Chin. J. Phys.* **74**, 421–439 (2021).
6. Rawat, S. K. & Kumar, M. Cattaneo–Christov heat flux model in flow of copper water nanofluid through a stretching/shrinking sheet on stagnation point in presence of heat generation/absorption and activation energy. *Int. J. Appl. Comput. Math.* **6**(4), 1–26 (2020).
7. Ciarletta, M. & Straughan, B. Uniqueness and structural stability for the Cattaneo–Christov equations. *Mech. Res. Commun.* **37**(5), 445–447 (2010).
8. Han, S., Zheng, L., Li, C. & Zhang, X. Coupled flow and heat transfer in viscoelastic fluid with Cattaneo–Christov heat flux model. *Appl. Math. Lett.* **38**, 87–93 (2014).
9. Ali, L., Ali, B., Liu, X., Ahmed, S. & Shah, M. A. Analysis of bio-convective MHD Blasius and Sakiadis flow with Cattaneo–Christov heat flux model and chemical reaction. *Chin. J. Phys.* (in press) (2021).
10. Ibrahim, W., Dessale, A. & Gamachu, D. Analysis of flow of visco-elastic nanofluid with third order slips flow condition, Cattaneo–Christov heat and mass diffusion model. *Propul. Power Res.* **10**(2), 180–193 (2021).
11. Raja, M. A. Z. *et al.* Cattaneo–Christov heat flux model of 3d hall current involving biconvection nanofluidic flow with Darcy-Forchheimer law effect: Backpropagation neural networks approach. *Case Stud. Therm. Eng.* **26**, 101168 (2021).
12. Ali, B., Hussain, S., Nie, Y., Hussein, A. K. & Habib, D. Finite element investigation of Dufour and Soret impacts on MHD rotating flow of Oldroyd-b nanofluid over a stretching sheet with double diffusion Cattaneo Christov heat flux model. *Powder Technol.* **377**, 439–452 (2021).

13. Lim, Y. J. *et al.* Von Kármán Casson fluid flow with Navier's slip and Cattaneo–Christov heat flux. *Case Stud. Therm. Eng.* **28**, 101666 (2021).
14. Salahuddin, T., Awais, M., Khan, M. & Altanji, M. Analysis of transport phenomenon in cross fluid using Cattaneo–Christov theory for heat and mass fluxes with variable viscosity. *Int. Commun. Heat Mass Transf.* **129**, 105664 (2021).
15. Mushtaq, A., Abbasbandy, S., Mustafa, M., Hayat, T. & Alsaedi, A. Numerical solution for Sakiadis flow of upper-convected Maxwell fluid using Cattaneo–Christov heat flux model. *AIP Adv.* **6**(1), 015208 (2016).
16. Stergios, G. Y. & Brian, G. H. Marangoni flows during drying of colloidal films. *Phys. Fluids* **18**(8), 082103 (2006).
17. Zhang, J.-G., Okano, Y. & Dost, S. Effect of radiative heat transfer on thermal-solutal Marangoni convection in a shallow rectangular cavity with mutually perpendicular temperature and concentration gradients. *Int. J. Heat Mass Transf.* **183**, 122104 (2022).
18. Yaseen, M., Rawat, S. K. & Kumar, M. Hybrid nanofluid (mos2-sio2/water) flow with viscous dissipation and Ohmic heating on an irregular variably thick convex/concave-shaped sheet in a porous medium. *Heat Transf.* **51**(1), 789–817 (2022).
19. Yaseen, M., Kumar, M. & Rawat, S. K. Assisting and opposing flow of a MHD hybrid nanofluid flow past a permeable moving surface with heat source/sink and thermal radiation. *Partial Diff. Equ. Appl. Math.* **4**, 100168 (2021).
20. Gumber, P., Yaseen, M., Rawat, S. K. & Kumar, M. Heat transfer in micropolar hybrid nanofluid flow past a vertical plate in the presence of thermal radiation and suction/injection effects. *Partial Diff. Equ. Appl. Math.* **5**, 100240 (2022).
21. Rawat, S. K., Negi, S., Upreti, H. & Kumar, M. A non-Fourier's and non-Fick's approach to study MHD mixed convective copper water nanofluid flow over flat plate subjected to convective heating and zero wall mass flux condition. *Int. J. Appl. Comput. Math.* **7**(6), 1–27 (2021).
22. Wang, T.-S. & Shi, W.-Y. Marangoni convection instability in an evaporating droplet deposited on volatile liquid layer. *Int. J. Heat Mass Transf.* **171**, 121055 (2021).
23. Jin, C., Okano, Y., Minakuchi, H. & Dost, S. Numerical simulation of thermo-solutal Marangoni convection in a full floating zone with radiative heat transfer under zero gravity. *J. Crystal Growth* **570**, 126204 (2021).
24. Sun, Y. S., Xu, J. Y., Wang, H. J., Hong, F. J. & Kita, H. Effects of natural and Marangoni convections on melting of high-temperature encapsulated phase change material under the earth and the moon gravities. *Appl. Therm. Eng.* **201**, 117760 (2022).
25. Li, Y. X. *et al.* Dynamics of aluminum oxide and copper hybrid nanofluid in nonlinear mixed Marangoni convective flow with entropy generation: Applications to renewable energy. *Chin. J. Phys.* **73**, 275–287 (2021).
26. Song, Y. Q. *et al.* Bioconvection analysis for Sutterby nanofluid over an axially stretched cylinder with melting heat transfer and variable thermal features: A Marangoni and solutal model. *Alexandria Eng. J.* **60**(5), 4663–4675 (2021).
27. Zhang, J.-G., Okano, Y. & Dost, S. Numerical simulation of Marangoni convection in a shallow rectangular cavity with a linear solutal boundary condition. *Int. J. Heat Mass Transf.* **178**, 121578 (2021).
28. Mahanthesh, B. Flow and heat transport of nanomaterial with quadratic radiative heat flux and aggregation kinematics of nanoparticles. *Int. Commun. Heat Mass Transf.* **127**, 105521 (2021).
29. Mackolil, J. & Mahanthesh, B. Heat transfer optimization and sensitivity analysis of Marangoni convection in nanoliquid with nanoparticle interfacial layer and cross-diffusion effects. *Int. Commun. Heat Mass Transf.* **126**, 105361 (2021).
30. Mackolil, J. & Mahanthesh, B. Inclined magnetic field and nanoparticle aggregation effects on thermal Marangoni convection in nanoliquid: A sensitivity analysis. *Chin. J. Phys.* **69**, 24–37 (2021).
31. Mackolil, J. & Mahanthesh, B. Sensitivity analysis of Marangoni convection in TiO2-EG nanoliquid with nanoparticle aggregation and temperature-dependent surface tension. *J. Therm. Anal. Calorim.* **143**(3), 2085–2098 (2021).
32. Mackolil, J. & Mahanthesh, B. Heat transfer enhancement using temperature-dependent effective properties of alumina-water nanoliquid with thermo-solutal Marangoni convection: A sensitivity analysis. *Appl. Nanosci.*, 1–12 (2021).
33. Mackolil, J. & Mahanthesh, B. Optimization of heat transfer in the thermal Marangoni convective flow of a hybrid nanomaterial with sensitivity analysis. *Appl. Math. Mech.* **42**(11), 1663–1674 (2021).
34. Kazemi, M. A., Saber, S., Elliott, J. A. & Nobes, D. S. Marangoni convection in an evaporating water droplet. *Int. J. Heat Mass Transf.* **181**, 122042 (2021).
35. Farooq, U., Waqas, H., Imran, M., Albakri, A. & Muhammad, T. Numerical investigation for melting heat transport of nanofluids due to stretching surface with Cattaneo–Christov thermal model. *Alexandria Eng. J.* **61**(9), 6635–6644 (2022).
36. Tiwari, R. K. & Das, M. K. Heat transfer augmentation in a two-sided lid-driven differentially heated square cavity utilizing nanofluids. *Int. J. Heat Mass Transf.* **50**(9–10), 2002–2018 (2007).
37. Chu, Y. M. *et al.* Cattaneo–Christov double diffusions (CCDD) in entropy optimized magnetized second grade nanofluid with variable thermal conductivity and mass diffusivity. *J. Mater. Res. Technol.* **9**(6), 13977–13987 (2020).
38. Anjum, A. *et al.* Physical aspects of heat generation/absorption in the second grade fluid flow due to Riga plate: Application of Cattaneo–Christov approach. *Results Phys.* **9**, 955–6 (2018).
39. AlQdah, K. S., Khan, N. M., Bacha, H. B., Chung, J. D. & Shah, N. A. Marangoni convection of dust particles in the boundary layer of Maxwell nanofluids with varying surface tension and viscosity. *Coatings* **11**(9), 1072 (2021).
40. Sheikholeslami, M., Ashorynejad, H. R., Domairry, G. & Hashim, I. Flow and heat transfer of cu-water nanofluid between a stretching sheet and a porous surface in a rotating system. *J. Appl. Math.*, **2012**, 18 (2012).
41. Ishak, A., Nazar, R. & Pop, I. Boundary layer flow and heat transfer over an unsteady stretching vertical surface. *Meccanica* **44**(4), 369–375 (2009).
42. Ganesh, N. V., Al-Mdallal, Q. M., Al Fahel, S. & Dadoa, S. Riga-plate flow of γ Al_2O_3-water/ethylene glycol with effective Prandtl number impacts. *Heliyon* **5**(5), e01651 (2019).

Acknowledgements

1. This Research was supported by Taif University Researchers Supporting Project Number (TURSP-2020/48), Taif University, Taif, Saudi Arabia. 2. The authors would like to thank the deanship of scientific research at Umm Al-Qura University for supporting this work by Grant Code: 22UQU4310392DSR04.

Author contributions

All persons who meet authorship criteria are listed as authors, and all authors certify that they have participated sufficiently in the work to take public responsibility for the content, including participation in the concept, design, analysis, writing, or revision of the manuscript. Furthermore, each author certifies that this material or similar material has not been and will not be submitted to or published in any other publication before its appearance in the Scientific Reports. Conception, Drafting and design of the study: N.M.K., K.A.M.A., N.U., M.N.A., K.M., A.A.A.M., S.A.

Competing interests

The authors declare no competing interests.

Additional information

Correspondence and requests for materials should be addressed to N.M.K.

Reprints and permissions information is available at www.nature.com/reprints.

Publisher's note Springer Nature remains neutral with regard to jurisdictional claims in published maps and institutional affiliations.